ADVANCED MATERIALS TECHNOLOGIES
www.advmattechnol.de

In-Situ Thermal Conductivity Modulation and Characterization of Silicon Carbide Nanowires via Bending Strain

Guangjie Gu, Yifan Fu, Zhen Li, Simin Yan, Zhanrui Jin, Shiqi He, Zijian Gao, Litao Sun, Meng Nie, and Kuibo Yin**

Silicon carbide (SiC) nanowires show great promise in advanced semiconductor applications, where internal stress generated during processing has a critical impact on their thermal conductivities. However, in situ stress modulation and thermal conductivity measurement of individual nanowires remain technically challenging. Herein, an in situ approach is proposed to characterize thermal transport of individual SiC nanowires under controlled bending strain utilizing Pt nanopillars on a MEMS suspended thermal bridge. Measurements reveal a 44.8% reduction in thermal conductivity at 0.429% bending strain, demonstrating a direct correlation between strain and phonon transport. Transmission electron microscopy confirms lattice deformation under bending, with compression on the inner arc and tension on the outer arc. Molecular dynamics simulations elucidate the physical mechanism of stress-induced thermal conductivity reduction. This work advances the understanding of strain-phonon scattering interactions in SiC nanowires and establishes a robust framework for in situ investigation of nanoscale thermal transport under mechanical stress, offering valuable insights for the design of strain-engineered semiconductor device.

1. Introduction

Silicon carbide (SiC) nanowires integrate the exceptional mechanical strength, chemical stability, and wide bandgap of bulk SiC with the quantum confinement and surface effects inherent to 1D nanostructures. This unique combination makes them a highly promising platform for next-generation semiconductor devices, high-power electronics, and thermal management systems.[1–3] However, practical applications of SiC nanowires are often hindered by internal stresses generated during device fabrication processes, such as those induced by mechanical bending, interfacial mismatch, or thermal cycling. Such stresses induce lattice deformation that significantly alters the nanowires' thermal conductivity, a critical parameter for heat dissipation and device reliability.[4,5] Despite the urgency to understand and regulate strain-dependent thermal transport in SiC nanowires, progress has been impeded by the experimental challenges in achieving in situ stress modulation coupled with nanoscale thermal conductivity measurements.[6]

Recent theoretical and simulation studies have provided preliminary insights into this strain-dependent thermal transport phenomenon. Guo et al.[7] predict a non-monotonic thermal conductivity trend in monolayer SiC under tensile strain via single-mode relaxation time approximation simulations, attributing this behavior to strain-dependent phonon lifetime variations. Wang et al.[8] demonstrated through non-equilibrium molecular dynamics (MD) that β-SiC exhibits a peak thermal conductivity at 4% compressive strain, governed by the interplay of phonon lifetime and group velocity. Contrastingly, Yin et al.[9] reported a monotonic decline in thermal conductivity for SiC nanowires under uniaxial strain, driven by reductions in phonon group velocity and specific heat. These conflicting theoretical predictions highlight the complexity of strain-phonon interactions in SiC nanostructures and underscore the need for experimental validation. To date, Cheng et al.[10] experimentally explored the relationship using the thermal bridge method, revealing that bent SiC nanowires exhibit reduced thermal conductivity due to strain-induced radial phonon scattering. Nevertheless, the absence of in situ strain regulation methodologies compatible with existing thermal characterization platforms has hindered systematic investigations of dynamic thermal transport behaviors under controlled deformation.

In this work, we utilize Pt nanopillars on a MEMS suspended thermal bridge structure to apply controlled bending strain to individual SiC nanowires and characterize their thermal conductivity under varying in situ bending stresses. Experiment results

G. Gu, Y. Fu, S. Yan, Z. Jin, S. He, Z. Gao, L. Sun, M. Nie, K. Yin
SEU-FEI Nano-Pico Center
Key Laboratory of MEMS of Ministry of Education
Southeast University
Nanjing 210096, P. R. China
E-mail: m_nie@seu.edu.cn; yinkuibo@seu.edu.cn

Z. Li
Jiangnan Key Laboratory of Advanced Food Manufacturing Equipment and Technology
School of Mechanical Engineering
Jiangnan University
Wuxi 214122, P. R. China

The ORCID identification number(s) for the author(s) of this article can be found under https://doi.org/10.1002/admt.202501529

DOI: 10.1002/admt.202501529

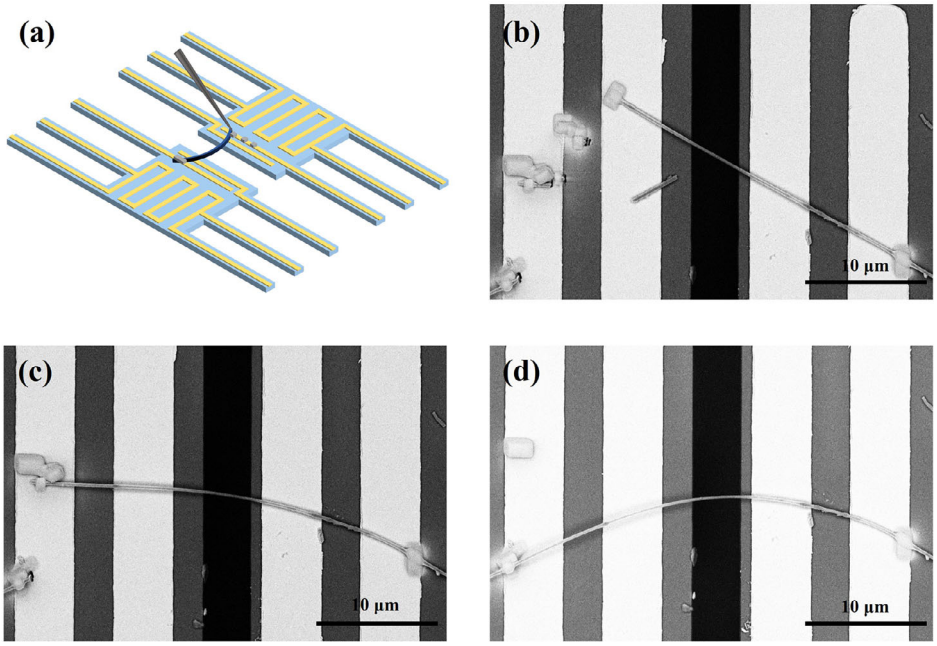

Figure 1. The in situ bending of SiC nanowire. a) The schematic diagram of the transferred SiC nanowire on the MEMS suspended thermal bridge device. b) SEM image of the straightening of a bending stress-free SiC nanowire. c,d) SEM images of the SiC nanowire with different bending degrees.

reveal a significant reduction in thermal conductivity with increasing bending strain, exhibiting a 44.8% decrease at a maximum normal strain of 0.429% and a maximum shear strain of 0.0154%. Transmission electron microscopy (TEM) analysis confirms lattice distortion featuring compressive stresses on the inner concave side and tensile stresses on the outer convex side of the bent nanowire. To ensure measurement accuracy, we adopt the electron beam self-heating method, which effectively mitigates systematic errors arising from interfacial thermal resistance at the electrode contacts. Additionally, molecular dynamics simulation further elucidate that the reduced thermal conductivity results from strain-induced radial phonon scattering. These findings not only introduce a novel in situ bending approach for investigating the strain-dependent thermal properties of SiC nanowires but also deepen the understanding of strain effects on nanoscale thermal transport, providing valuable insights for the design of next-generation semiconductor devices.

2. Results and Discussion

Figure 1a shows the schematic diagram of the transferred SiC nanowire on the MEMS suspended thermal bridge device. The serpentine resistor exhibits a linear temperature-resistance relationship, with its temperature coefficient α determined as 2.064 $\times 10^{-3}$ Ω K^{-1} using a calibrated oven coupled to a Delta measurement system. Subsequently, Pt nanopillars (approximate dimensions: 1 × 0.5 × 0.5 μm) were fabricated at predefined locations on a separate suspended platform to serve as bending support points. A nanomanipulator probe system was employed to establish contact with the free end of the nanowire, which was then sequentially anchored to different Pt nanopillars, enabling controlled bending to various angles. Representative transfer results are shown in Figure 1b–d. At each bending state (including the initial configuration), in situ thermal conductivity measurements were systematically conducted to evaluate strain-dependent thermal transport properties. The thermal characterization was performed using a non-contact electron beam self-heating technique based on localized energy deposition through electron-phonon interactions. This method utilizes a focused electron beam as a heat source while measuring temperature responses through integrated platinum thermometers, effectively eliminating interfacial thermal resistance.[11] Theoretical calculations confirm that our applied acceleration voltage (5 kV) is significantly below the critical threshold for atomic displacement damage (110–258 kV),[12–14] ensuring that the measured thermal properties reflect intrinsic material behavior rather than beam-induced artifacts. The electron beam energy is primarily dissipated through controlled thermal effects while preserving the structural integrity of the nanowires.

The thermal conductivity k of the SiC nanowires was calculated using Equation (1),[15,16]

$$k = \frac{1}{\frac{\mathrm{d}R_i(x)}{\mathrm{d}x} \times A} \tag{1}$$

where $R_i(x)$ represents the distribution function of the thermal resistance of the SiC nanowire along its length, and A is the cross-sectional area of the SiC nanowire, as determined from SEM characterization images.

The measured thermal conductivity of the pristine SiC nanowire is ≈11 $Wm^{-1}K^{-1}$, as shown in **Figure 2**, which is consistent with values reported in previous studies.[7,17] For SiC nanowire Sample 1, the thermal conductivity decreases from 11 (straight) to 8.13 W $m^{-1}K^{-1}$ (bent), corresponding to a 26.1% reduction, as the bending curvature increases. Concurrently, the normal strain reaches 0.421% and the shear strain 0.0025%. For

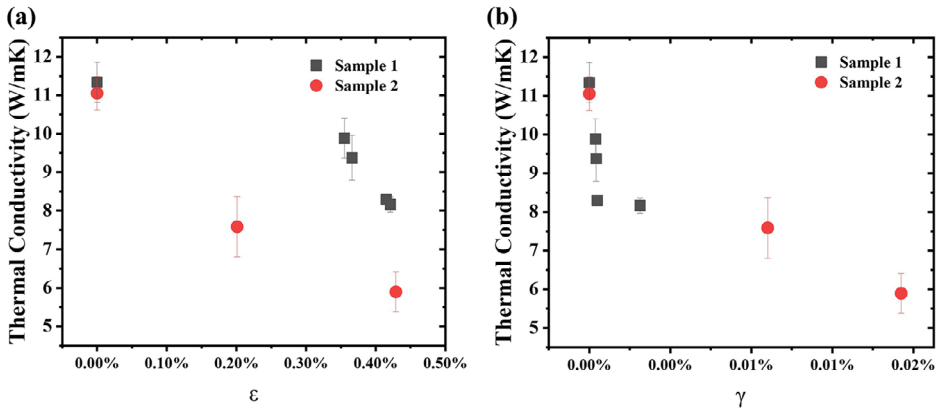

Figure 2. Relationship between strain and thermal conductivity. a) Relationship between normal strain and thermal conductivity. b) Relationship between shear strain and thermal conductivity.

SiC nanowire Sample 2, the thermal conductivity decreases from 10.7 (straight) to 5.9 W $m^{-1}K^{-1}$ (bent), corresponding to a 44.8% reduction, with the normal strain reaching 0.429% and the shear strain 0.0154%. The results demonstrate that the thermal conductivity of SiC nanowires decreases with increasing bending strain.

The lattice thermal conductivity in classical dynamics is given by:[18]

$$\kappa = \frac{1}{3} Cvl \tag{2}$$

Equation (2) shows that the thermal conductivity of crystals is directly proportional to three key phonon parameters: the phonon specific heat capacity (C), the phonon group velocity (v), and the phonon mean free path (l), where $l = v\tau$ (τ denotes the relaxation time).

From the perspective of heat transport mechanisms, long-wavelength phonons dominate thermal transport processes. The value of the C is primarily determined by the phonon density of states. Although strain induces shifts in the phonon spectrum (compressive strain increases frequencies while tensile strain decreases them),[8] the integrated contribution of these frequency changes to the heat capacity is minimal within our experimental temperature range. At room temperature, C is near the Dulong-Petit limit and minimally affected by strain. Therefore, the modulation of heat capacity by strain gradients is not the dominant factor in the observed thermal conductivity variation. The v is directly related to the slope of the phonon dispersion relation. Theoretical studies confirm that tensile strain reduces the group velocity of acoustic phonons through phonon spectrum "softening", while compressive strain may enhance it via "hardening" effects.[9] In bent nanowires, the strain gradient causes a net v reduction. Shear strain further lowers v via mode coupling. Although the coexistence of compressive and tensile regions in the bent nanowires creates a complex net effect, the alteration in group velocity remains an important aspect for understanding strain effects. It is concluded that the primary factor responsible for thermal conductivity reduction is the strong suppression of the l by strain gradients. The bending-induced strain gradient creates a continuously varying scattering potential field, which not only causes phonon spectrum broadening[10] and increases the scattering phase space, but also directly enhances phonon-phonon interactions. It leads to a sharp decrease in τ,[19] consequently reducing the mean free path.

As illustrated in **Figure 3**a, the normal stress is compressive on the nanowire's concave side and tensile on its convex side. In a uniform nanowire, compressive and tensile stresses are theoretically distributed symmetrically across the cross-section. Theoretical analyses indicate that thermal conductivity increases linearly as the stress state shifts from tensile to compressive. However, normal stress alone cannot fully account for the significant thermal conductivity reduction observed in bent nanowires.[20] In contrast, shear stress (defined as the stress component coplanar with the nanowire's cross-section plane) induces cross-sectional warping, which subsequently affects thermal conductivity. The deformation establishes an intermediate layer within the beam, referred to as the neutral layer. The intersection of this layer with the beam's cross-section forms the neutral axis.[21] During bending, each cross-section rotates about its neutral axis. In planar bending, the neutral axis remains perpendicular to the cross-section's vertical symmetry axis. The normal stress magnitude at any point on the cross-section varies linearly with its distance from the neutral axis, with tensile stresses dominating on one side and compressive stresses on the opposing side. Combining this stress distribution with the strain law for beam bending yields the normal stress formula:

$$\sigma = \frac{M}{I_z} y \tag{3}$$

The maximum stress is as follows:

$$\sigma = \frac{M_{max}}{I_z} y_{max} = \frac{M_{max}}{W_z} \tag{4}$$

where I_z is the moment of inertia about the neutral axis z, W_z is the flexural section modulus about axis z, and the bending moment M is given by:[21,22]

$$M = \frac{E}{\rho} \int y^2 dA \tag{5}$$

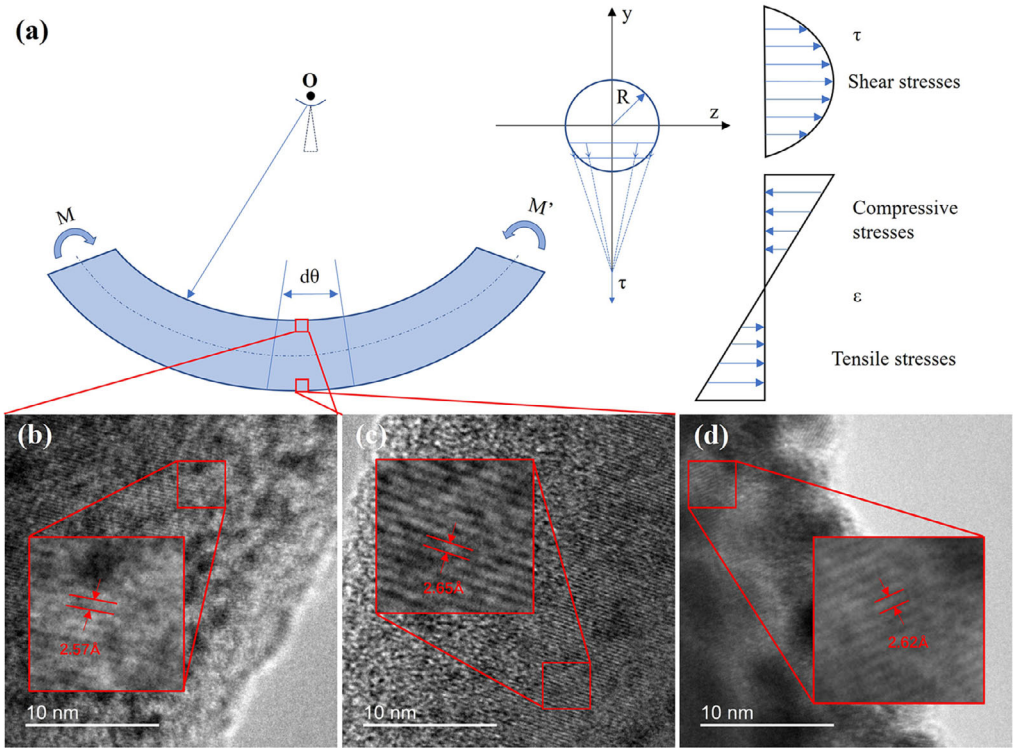

Figure 3. Stress analysis of bent nanowires and TEM characterization of bent and straightened SiC nanowires. a) Schematic diagram of stress analysis for bent nanowires. b) The outer side of the bent SiC nanowires. c) The inner side of the bent SiC nanowires. d) The straight SiC nanowires.

where E is Young's modulus, ρ is the radius of curvature of the neutral surface, y is the distance to the neutral surface, and A is the cross-sectional area. For a cylindrical beam:

$$l_z = \frac{\pi D^4}{64} \tag{6}$$

$$W_z = \frac{\pi D^3}{32} \tag{7}$$

The strain caused by normal stress is:

$$\varepsilon = \frac{y}{\rho} \tag{8}$$

The shear stress τ of the cross-section is:

$$\tau = \frac{dM}{dx} \times \frac{1}{\pi R^2} \tag{9}$$

The shear strain γ is:

$$\gamma = \frac{\tau}{G} \tag{10}$$

where G is the shear modulus. For SiC nanowires, the values used are E = 448 GPa (Young's modulus) and G = 192 GPa (shear modulus), as reported in the literature.[23]

Beyond modulating lattice thermal conductivity through regulating the phonon mean free path, stress induces microstructural modifications, including grain boundary defects[24,25] and lattice distortions.[26] These imperfections disrupt the crystalline periodicity, enhancing lattice anharmonicity and further degrading thermal transport. TEM micrographs in Figure 3b–d systematically compare the morphology of bent and straight nanowires. HRTEM images reveal three distinct characteristic regions: compressed inner arc, tensile outer arc, and a straightened reference region at identical cross-sectional positions. Quantitative analysis reveals lattice spacings of 2.57 ± 0.02 Å (inner, Figure 3c), 2.65 ± 0.02 Å (outer, Figure 3b), and 2.62 ± 0.01 Å (straightened, Figure 3d), respectively. The compressed region exhibits a reduced lattice spacing relative to the tensile outer region, with unbent nanowires exhibiting intermediate values. Consistent results were obtained for Sample 2, confirming bending-induced lattice geometry modifications.

Building on this, the influence of the strain gradient on long-wavelength phonons—the dominant heat carriers—manifests primarily in two aspects. First, it modulates the phonon dispersion relations: compressive regions induce phonon spectrum "hardening" (frequency increase), while tensile regions cause "softening" (frequency decrease).[8] This spatial heterogeneity affects the group velocity of acoustic phonons. However, the more critical mechanism lies in the pronounced effect of the strain gradient on phonon lifetime. The gradient strain field leads to a general broadening of the phonon dispersion,[10] which substantially increases the number of phonon scattering channels satisfying energy and momentum conservation (i.e., enlarging the scattering phase space). This strongly enhances phonon-phonon scattering, significantly reducing phonon lifetime and mean free path.[9] The decline in thermal conductivity observed in the MD

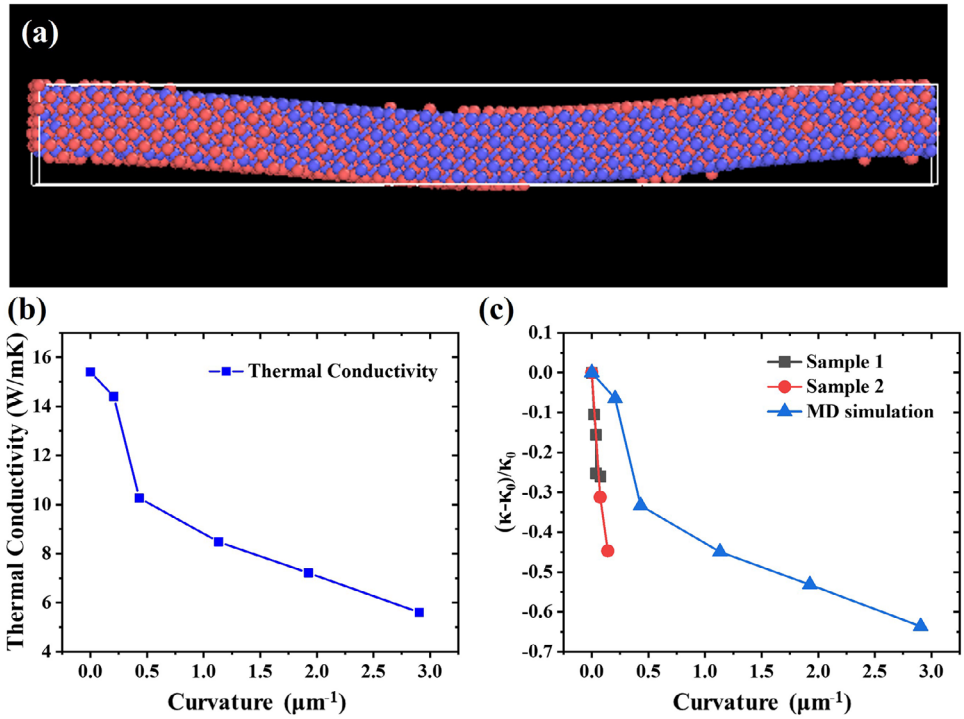

Figure 4. a) MD-simulated bent SiC nanowires. b) Variation of thermal conductivity of SiC nanowires with bending degree in MD simulation. c) Comparison of thermal conductivity between experimental results and MD-simulated bent SiC nanowires.

simulations is a macroscopic manifestation of this scattering enhancement mechanism, leading to shortened mean free paths. It should be noted that this effect exhibits significant mode dependence. Acoustic phonons, particularly long-wavelength acoustic modes, as the primary heat carriers, play a decisive role in determining thermal conductivity through alterations in their properties. In contrast, optical phonons, due to their relatively minor contribution to heat transport, exert a comparatively secondary influence.[27]

To further elucidate the mechanism underlying stress-induced thermal conductivity reduction in SiC nanowires, MD simulations were performed to systematically evaluate thermal transport across bending configurations. As shown in **Figure 4**, the results reveal a monotonic decrease in thermal conductivity with increasing bending curvature, consistent with theoretical models based on phonon density of states (DOS) analysis. The key mechanism involves strain-induced broadening of the phonon DOS.[28] Figure 2 in Ref. [28] illustrates this broadening effect on the phonon spectrum in an atomic chain under a strain gradient, comparing the frequency distribution under different gradient magnitudes. The broadening effect significantly increases the phase space for phonon-phonon scattering, enabling more scattering processes to satisfy energy and momentum conservation conditions, thereby strongly enhancing the scattering rate.[9] The direct consequence is a notable reduction in phonon lifetime and mean free path, which effectively explains the thermal conductivity decrease observed in the simulations of the manuscript. It is important to emphasize that the DOS of low-frequency acoustic phonons is particularly sensitive to strain,[7] and as the primary heat carriers, their property changes play a decisive role in thermal conductivity variation. For computational efficiency, the MD model was scaled down to 13.59 Å (length) × 13.03 Å (width) × 165.01 Å (height), preserving geometric similarity to experimental specimens. The pristine nanowire model exhibits 15.97 W $m^{-1}K^{-1}$ thermal conductivity, decreasing by 64.6% to 5.66 W m^{-1} K^{-1} under maximum bending. While this trend qualitatively aligns with the experimental observations, the simulated reduction magnitude is less pronounced.

3. Conclusion

In summary, this study presents a systematic investigation of stress-induced thermal transport modulation in SiC nanowires through an integrated approach combining experiments and computations. In situ thermal bridge measurements, coupled with contact resistance compensation via the electron beam self-heating technique, demonstrate a maximum thermal conductivity reduction of 44.8% during bending. HRTEM lattice analysis confirms the formation of a strain gradient, characterized by a lattice spacing variation of 2.58–2.65 Å between compressive inner and tensile outer arcs. MD simulations quantitatively corroborate the experimental trends, attributing the thermal conductivity degradation to strain-enhanced lattice anharmonicity. Mechanistically, stress-mediated bond distortion activates additional phonon modes while intensifying Umklapp scattering, thereby collectively suppressing heat transport. These findings establish fundamental principles for strain-mediated phonon engineering, providing critical mechanistic insights for advancing the development of high-efficiency thermoelectric materials.

4. Experimental Section

The MEMS suspended thermal bridge device consists of two suspended silicon nitride (SiN) platforms, each integrated with a platinum (Pt) serpentine resistor that serves dual functions as both a heater and a temperature sensor. Mechanical support and electrical interconnection are provided by six Pt/SiN composite cantilevers, which anchor each suspended platform while routing signals from the serpentine resistors and the integrated electrodes.[29–32] The structural features of the MEMS suspended thermal bridge device and SiC nanowires were examined using a dual-beam system (Helios 5CX) combining focused ion beam (FIB) and scanning electron microscopy (SEM). A four-probe configuration, implemented with a Delta measurement system (including a Keithley 6221 current source and a Keithley 2182 nanovoltmeter), was employed to record the resistance-temperature relationship of the Pt serpentine resistors. All measurements were conducted in a high-vacuum chamber ($<10^{-4}$ Pa) to eliminate thermal interference from air conduction and convection. The lattice structure of strained SiC nanowires was analyzed using high-resolution transmission electron microscopy (HRTEM, TECNAI G2 20) to correlate bending-induced lattice defects with thermal transport properties.

The SiC nanowires used in this study were procured from Jiangsu XFNANO Materials Tech Co., Ltd., with a purity of 98%. The experimental procedure began with the transfer of SiC nanowire to a MEMS suspended thermal bridge device via a tungsten probe-assisted manipulation technique. The device with the transferred nanowire was subsequently loaded into the Helios 5CX system. Within the dual-beam chamber, electron beam-induced deposition (EBID) was utilized to deposit Pt anchoring blocks at the nanowire ends on the suspended platform, thereby ensuring mechanical stability during subsequent bending operations.

Acknowledgements

The authors acknowledge the funding provided by the National Key R&D Program of China (Grant No. 2024YFA1207900), the National Natural Science Foundation of China (Grant Nos. 12174050 and 62274031), Basic Research Program of Jiangsu (Grant No. BK20243023), Jiangsu Provincial Natural Science Foundation of China (Grant No. BK20231411).

Conflict of Interest

The authors declare no conflict of interest.

Data Availability Statement

The data that support the findings of this study are available from the corresponding author upon reasonable request.

Keywords

bending strain, in situ characterization, silicon carbide nanowire, strain engineering, thermal conductivity modulation

Received: July 18, 2025
Revised: September 29, 2025
Published online:

[1] M. S. I Islam, N. Ferdous, J. Park, A. Hashimoto, *Phys. Chem. Chem. Phys.* **2020**, *22*, 13592.
[2] M. S. Islam, A. Islam, O. Mahamud, A. Saha, N. Ferdous, J. Park, A. Hashimoto, *AIP Adv.* **2020**, *10*, 015117.
[3] M. White, National Science Foundation (NSF) project. Grant No. 0207093, **2002**.
[4] H. K. Seong, H. J. Choi, S. K. Lee, J. I. Lee, D. J. Choi, *Appl. Phys. Lett.* **2004**, *85*, 1256.
[5] J. Wei, X. T. Li, Y. Wang, B. Chen, M. J. Zhang, C. M. Qin, *J. Am. Ceram. Soc.* **2020**, *103*, 6187.
[6] K. Rogdakis, S. Y. Lee, M. Bescond, S. K. Lee, E. Bano, K. Zekentes, *IEEE Trans. Electron Devices* **2008**, *55*, 1970.
[7] S. D. Guo, J. Dong, J. T. Liu, *Phys. Chem. Chem. Phys.* **2018**, *20*, 22038.
[8] Y. H. Wang, B. Q. Fu, *J. Mater. Res.* **2023**, *38*, 1634.
[9] K. L. Yin, L. P. Shi, X. L. Ma, Y. S. Zhong, M. W. Li, X. D. He, *Nanomaterials* **2023**, *13*, 2196.
[10] W. K. Chen, X. S. Wu, S. C. Deng, N. Yang, X. F. Xu, *Appl. Phys. Lett.* **2024**, *124*, 242201.
[11] D. Liu, R. Xie, N. Yang, B. Li, J. T. L. Thong, *Nano Lett.* **2014**, *14*, 806.
[12] M. Shur, S. Rumyantsev, M. E. L. J., *World Sci.* **2007**, *14*, 921.
[13] C. Kasper, D. Klenkert, Z. Shang, D. Simin, A. Gottscholl, A. Sperlich, H. Kraus, C. Schneider, S. Zhou, M. Trupke, W. Kada, T. Ohshima, V. Dyakonov, G. V. Astakhov, *Phys. Rev. Appl.* **2020**, *13*, 044054.
[14] D. B. Williams, C. Barry Carter, *Transmission Electron Microscopy: A Textbook for Materials Science*, Springer, USA **2009**.
[15] Z. Q. Wang, R. G. Xie, C. T. Bui, D. Liu, X. X. Ni, B. W. Li, J. T. L. Thong, *Nano Lett.* **2011**, *11*, 113.
[16] S. Y. Lee, W. Y. Lee, J. T. L. Thong, G. S. Kim, S. K. Lee, *Nanotechnology* **2016**, *27*, 115402.
[17] L. A. Valentín, J. Betancourt, L. F. Fonseca, M. T. Pettes, L. Shi, M. Soszynski, A. Huczko, *J. Appl. Phys.* **2013**, *114*, 184301.
[18] P. G. Klemens, *Solid State Phys.* **1958**, *7*, 1.
[19] X. Liu, H. Zhou, G. Zhang, Y.-W. Zhang, *J. Appl. Phys.* **2019**, *125*, 082505.
[20] J. Huang, Y. F. Zhang, A. R. Fan, Y. P. Li, H. D. Wang, W. G. Ma, X. Zhang, *ACS Appl. Mater. Interfaces* **2023**, *15*, 39689.
[21] H. Y. Huang, G. A. Kardomateas, *AIAA J.* **2002**, *40*, 2331.
[22] J. N. Reddy, C. M. Wang, K. H. Lee, *Int. J. Solids Struct.* **1997**, *34*, 3373.
[23] W. X. Li, T. C. Wang, *Phys. Rev.* **1999**, *59*, 3993.
[24] D. S. Kim, O. Hellman, N. Shulumba, C. N. Saunders, J. Y. Y. Lin, H. L. Smith, J. E. Herriman, J. L. Niedziela, D. L. Abernathy, C. W. Li, B. Fultz, *Phys. Rev.* **2020**, *102*, 174311.
[25] Y. G. Zhou, M. Hu, *Nano Lett.* **2016**, *16*, 6178.
[26] X. D. Han, Y. F. Zhang, K. Zheng, X. N. Zhang, Z. Zhang, Y. J. Hao, X. Y. Guo, J. Yuan, Z. L. Wang, *Nano Lett.* **2007**, *7*, 452.
[27] G. Jiao, S. Qiao, J. Lyu, Y. Tao, L. Yang, *Phys. Rev. Appl.* **2024**, *22*, 054019.
[28] L. Yang, S. Yue, Y. Tao, S. Qiao, H. Li, Z. Dai, B. Song, Y. Chen, J. Du, D. Li, P. Gao, *Nature* **2024**, *629*, 1021.
[29] L. Shi, D. Y. Li, C. H. Yu, W. Y. Jang, D. Y. Kim, Z. Yao, P. Kim, A. Majumdar, *J. Heat Transfer-Transact. ASME* **2003**, *125*, 1209.
[30] Q. L. Wang, X. Liang, B. H. Liu, Y. H. Song, G. H. Gao, X. F. Xu, *Nanoscale* **2020**, *12*, 1138.
[31] Y. S. Zhao, D. Liu, J. Chen, L. Y. Zhu, A. Belianinov, O. S. Ovchinnikova, R. R. Unocic, M. J. Burch, S. Kim, H. F. Hao, D. S. Pickard, B. W. Li, J. T. L. Thong, *Nat. Commun.* **2017**, *8*, 15919.
[32] S. F. Karg, V. Troncale, U. Drechsler, P. Mensch, P. D Kanungo, H. Schmid, V. Schmidt, L. Gignac, H. Riel, B. Gotsmann, *Nanotechnology* **2014**, *25*, 305702.